

# A Comprehensive Performance Analysis for mm-Wave Massive MIMO Hybrid Beamforming under PA Nonlinearities

Murat Babek Salman, *Student Member, IEEE*,

Gokhan Muzaffer Guvensen, *Member, IEEE*,

## Abstract

In this paper, we develop a framework to investigate the performances of different hybrid beamforming architectures for massive multiple input multiple output (MIMO) systems impaired by power amplifier (PA) nonlinearities. Indirect learning architecture based on feedback after anti-beamforming is adopted in design of digital pre-distortion (DPD) in order to compensate the nonlinear distortion caused by PA. In addition, we propose a novel analog beamformer design for partially connected architecture based on generalized eigen-beamformer (GEB) approach. In literature, the effects of nonlinear PA's on the out-of-band (OOB) radiation and achieved signal-to-interference-plus-noise ratio (SINR) are investigated. However, these studies are limited to fully digital or partially connected hybrid beamforming architectures while deploying Bussgang decomposition on a PA basis without considering the array architecture type in performance analysis. In this study, we derived an analytical bit-error-rate (BER) expression based on spatio-temporal Bussgang decomposition in matrix form, and mismatched decoding

M. B. Salman is with the Department of Electrical and Electronics Engineering, Middle East Technical University, Ankara, 06800 Turkey e-mail: mbsalman@metu.edu.tr.

G. M. Guvensen is with the Department of Electrical and Electronics Engineering, Middle East Technical University, Ankara, 06800 Turkey e-mail: guvensen@metu.edu.tr.

capacity via Generalized Mutual Information (GMI) is obtained under PA nonlinearity for different hybrid Massive MIMO architectures. Analytical results show that the nonlinear distortion significantly affects the system performance, and DPD can reduce these effects to some extend. Finally, obtained analytical BER expression is verified via numerical results.

### Index Terms

Massive MIMO, hybrid beamforming, nonlinear distortion, performance analysis, digital pre-distortion.

## I. INTRODUCTION

Multiple-input multiple-output (MIMO) systems operating at millimeter-wave (mm-Wave) frequencies are expected to meet constantly growing data rate requirements that cannot be met by current systems [1]–[4]. Radio signals, at mm-Wave frequencies, are exposed to severe absorption losses [1], [2]. Large scale antenna arrays, also called as massive MIMO systems, are used to increase the multiplexing gain so that effects of these losses are reduced [3], [5]. On the other hand, using a large number of antennas has certain limitations. In conventional MIMO systems, which are employed for sub-6 GHz frequency bands, fully digital precoding can be implemented; however, doing so is quite costly for massive MIMO systems due to need of excessive number of RF chains which consume immense amount of power [6]–[8]. Massive MIMO transceivers are equipped with low-cost highly-efficient nonlinear power amplifiers (NPA)’s to reduce the implementation cost, consequently, transmitted signal suffers from nonlinear distortion.

In order to reduce power consumption and implementation complexity, hybrid beamforming based array architectures have been developed. In these architectures, beamforming is divided into two stages, where precoding is performed in digital domain and analog beamformer connects  $D$  RF chains to  $N_t$  transmit antennas for  $D < N_t$ . One common approach is to implement analog beamformer as a partially connected architecture, where each RF chain is connected to a subarray composed of a series of phase shifters [9]. Then, digital precoder is designed based

on the reduced dimensional effective channel. Joint spatial division and multiplexing (JSDM) is also proposed as a two stage beamforming framework [10]. In JSDM, analog beamformer is designed based on spatial characteristics of the channels of users, which are characterized by their channel covariance matrices (CCM)'s. In addition, users having similar CCM's are grouped together so that they can be jointly processed in digital domain. Analog beamformer is designed to eliminate inter-group interferences and distinguishes signals of different groups. Digital precoder, on the other hand, is designed based on instantaneous channel in reduced dimension to suppress intra-group interference. In [11], [12], fully connected generalized eigen beamformer (GEB) is proposed as a statistical analog beamformer, which is shown to be optimal for several criteria. In proposed GEB, sub-beamformers are formed for each group such that beampattern contains deep nulls for angular sectors of other groups. This type of beamformer is suitable for the wideband massive MIMO channel, which is expected to be sparse both in the angle and delay domains [13].

In massive MIMO systems, low-cost PA's operating close to saturation are considered to be employed in future 5G systems in order to increase the power efficiency [14]. PA's exhibit nonlinear characteristics in that region; consequently, transmitted signal is nonlinearly distorted. In this paper, we investigate the effects of PA nonlinearities on mm-wave Massive MIMO systems and examine compensation methods for such effects.

Nonlinear distortion affects the system performance in several aspects, which are studied in literature [15]–[22]. In [15]–[17], out-of-band (OOB) radiation of massive MIMO systems are investigated with a particular focus on spatial characteristics of the radiation and a framework is developed for such analysis. These works consider fully digital beamforming and states that distortion effects are reduced as the number of antennas increases. Also, it was shown that as the number of users increases distortion power becomes isotropic and worst case happens, when a single user is present, where distortion is also concentrated towards that user. In [18], [23], hybrid beamforming architecture is considered and both OOB radiation pattern and digital predistortion

(DPD) techniques are studied. Different DPD design methods are proposed based on single PA feedback and anti-combining feedback architectures. It was shown that OOB radiation can be significantly reduced by DPD per RF chain. However, in [24] we showed that DPD per RF chain cannot mitigate OOB radiation problem for fully connected hybrid architecture. Since, input of each PA is the combination of all RF chains, DPD per RF chain is not sufficient for such structure.

Furthermore, effects of nonlinear distortion on the capacity and error probability of the system are studied in [19]–[22], [25]. In [19], [25], analysis on achievable information rate (AIR) is presented showing that capacity of massive MIMO systems is significantly reduced. However, these studies consider the spectral efficiency in terms of unconstrained Shannon capacity and system is limited to be fully digital. In [24], we extended analysis to a more general framework where constraint mismatch generalized mutual information (GMI) metric, which is presented in [26]–[29], is adopted to evaluate the performance of the system where fully connected hybrid architecture is adopted. In literature, in addition to capacity analysis, bit/symbol error probability (BER/SER) performances of fully digital massive MIMO systems are investigated by using narrowband Bussgang decomposition per antenna (scalar Bussgang with no frequency selectivity). In [20]–[22], both numerical and analytical BER/SER analysis are presented. It was shown that nonlinear distortion significantly increases BER of the system. Moreover, in [30], a signal-to-interference-plus-noise ratio (SINR) expression based on memory polynomial (MP) model is presented.

#### A. Contributions

In this paper, an extensive performance comparison between different massive MIMO array beamforming structures under PA non-linearity are carried out through complete analysis when proper DPD at BS or post-equalization at user side is utilized. A general analysis framework, covering different massive MIMO array types such as fully digital, fully connected hybrid /

partially connected hybrid architectures, is proposed in order to quantify the performance losses in terms of radiation patterns, AIR, and BER under PA non-linearities for multicarrier downlink transmission with higher order QAM constellations. To the authors knowledge, in the recent literature, there is no such a comprehensive analytical investigation and comparison made before.

Under the proposed framework, the contribution is two-fold. First, the nonlinearity due to PAs is modeled via vectorial wideband Bussgang decomposition in spatio-frequency domain, while taking the effect of hybrid beamforming structure into account. That is to say, the nonlinear system, from RF chain inputs including DPD units to PA outputs following the analog beamformer, is modeled in upsampled multidimensional signal domain. Here, the proposed modeling considers the spatial correlation among different transmit antennas at different subcarriers due to hybrid massive MIMO structure and PA memory.

Second, based on the general spatio-frequency Bussgang decomposition, peculiar to hybrid array connection type, BER and AIR analysis are fulfilled for different conventional DPD techniques (based on memory polynomial model [31]) and post frequency compensation methods at user terminal (UT). The effect of different beamforming types on the BER is demonstrated clearly both via the simulation and provided analysis. Moreover, mismatched decoding capacity via Generalized Mutual Information (GMI) is exploited to find a lower bound for AIR in case of mismatches (depending on array architecture) due to nonlinearity. It is observed that the hybrid array connection type is highly effective on the success of DPD and radiation patterns.

As a side contribution, a novel GEB based partially connected subarray structure is proposed in order to compromise between the out-of-band-radiation (OOB) pattern, nulling performance and BER.

## II. SYSTEM MODEL

In the considered system, a base station, which is equipped with  $D$  RF chains and  $N_t$  antennas, serves  $U$  single antenna users in time domain duplex (TDD) mode so that channel reciprocity

can be exploited. Assuming a block fading frequency selective channel which is slowly varying compared to signalling interval, received signal at the  $u^{th}$  user can be given in time domain as,

$$r_n^{(u)} = \sum_{l=0}^{L-1} [\mathbf{h}_l^{(u)}]^H \mathbf{y}_{n-l} + \nu_n^{(u)}. \quad (1)$$

In (1),  $r^{(u)}$  is the received signal,  $\mathbf{h}_l^{(u)} \in \mathbb{C}^{N_t \times 1}$  is the  $l^{th}$  delay of the channel impulse response of the  $u^{th}$  user and  $\mathbf{y}_n \in \mathbb{C}^{N_t \times 1}$  is the transmitted signal, which is corrupted by the non-linear PA.  $\nu^{(u)}$  is the additive white Gaussian noise (AWGN) with variance  $N_o$ .

#### A. mm-Wave Wideband Massive MIMO Channel Model

In this study, channel under consideration is taken to be sparse in both angular and temporal domains since massive MIMO systems are considered for millimeter (mm) wave frequencies, where channel sparsity is pronounced. By exploiting sparsity, multipath components stemming from the same angular sector can be grouped together so that JSDM can be used to reduce effective dimension of the problem. In JSDM framework, users that reside in the same angular sector can be processed jointly since they share similar spatial statistics. Users are partitioned into several groups and multipath components (MPC)'s of the users in the same group are composed of uncorrelated rays which are locally scattered according to wide sense stationary uncorrelated scattering (WSSUS) model [10]. According to this model, MPC's belonging the same group have the same channel covariance matrix (CCM),  $\mathbf{R}_l^{(g)} \in \mathbb{C}^{N_t \times N_t}$ , which can be expressed according to one-ring scattering model as,

$$\mathbf{R}_l^{(g_u)} = \frac{\gamma_l^{(g)}}{2\Delta} \int_{\theta_c^{g,l}-\Delta}^{\theta_c^{g,l}+\Delta} \mathbf{a}(\theta) [\mathbf{a}(\theta)]^H d\theta, . \quad (2)$$

where  $\gamma_l^{(g)}$  is the gain of the corresponding channel, which can also be inferred as power delay profile (pdp), and  $Tr\{\mathbf{R}_l^{(g)}\} = \gamma_l^{(g)}$ .  $\theta_c^{g,l}$  is the center of the angular sector of  $l^{th}$  MPC of the group  $g$ ,  $\mathbf{a}(\theta)$  is the unit norm steering vector for the azimuth angle  $\theta$ .  $l^{th}$  MPC of the  $u^{th}$  user of the  $g^{th}$  group is distributed as  $\mathbf{h}_l^{g_u} \in \mathbb{C}^{N \times 1} \stackrel{\text{i.i.d.}}{\sim} \mathcal{C}(\kappa^{(g,l)} \mathbf{a}(\theta_c^{g,l}), \mathbf{R}_l^{(g)})$ . In the given channel model, it is assumed that MPC is Rician distributed where a strong MPC exists at the center of the

angular center with Rician factor,  $\kappa^{(g,l)}$ . Then, received signal of the  $u^{th}$  user of the  $g^{th}$  group can be expressed as  $r_n^{(g_u)} = \sum_{l=0}^{L_g-1} [\mathbf{h}_l^{(g_u)}]^H \mathbf{y}_{n-l} + \nu_n^{(g_u)}$ . Besides, it is assumed that instantaneous channel state information (CSI) is acquired perfectly during the training period.

### B. Nonlinear PA Distortion

In order to study the effects of the PA nonlinearities on the performance of the hybrid beamforming system, modelling the nonlinear PA is mandatory. Output of the nonlinear PA can be expressed in terms of the basis functions as,

$$y_n^{(m)} = \sum_{\varpi=-\Pi+1}^{\Pi-1} \sum_{v=0}^{\Upsilon-1} \alpha_{\varpi,v}^m \phi_{\varpi,v}(\bar{x}_{n-\varpi}^{(m)}), \quad (3)$$

where  $y_n^{(m)}$  is the transmitted signal at the  $m^{th}$  antenna branch,  $\phi_{\varpi,v}(\cdot)$  are the basis functions,  $\bar{x}_{n-\varpi}^{(m)}$  is the input of nonlinearity and  $\alpha$ 's are the basis coefficients. The basis functions can be any function such as Memory Polynomial (MP) [31] or Hermite Polynomials [17] basis. For simplicity, in this work we consider MP expansion where the basis functions are  $\phi_{\varpi,v}(\bar{x}_{n-\varpi}) = \bar{x}(n-\varpi)|\bar{x}(n-\varpi)|^{2v}$ .

## III. A GENERIC TRANSMISSION SCHEME

A generic transmitter structure based on hybrid beamforming architecture is shown in Fig. 1. In the considered structure,  $U$  users are grouped into  $G$  groups, each having  $U_g$  users. In addition,  $D_g$  RF chains are assigned to each group,  $\sum_{g=1}^G D_g = D$ , where  $D < N_t$  is the total number of available RF chains. Main motivation behind the use of hybrid beamforming is that reduced number of RF chains is sufficient in hybrid structure as opposed to fully digital structure, which requires as many RF chains as the number of antennas. Even though, the considered structure defines a hybrid beamforming architecture, it is easily extended to fully digital architecture as  $G = 1$  and  $D = N_t$ . Then, the transmitted signal can be formed by utilizing OFDM modulation as,

$$\bar{\mathbf{x}}_n = \frac{1}{\mu K} \sum_{k=0}^{\mu K-1} \mathbf{B} \mathbf{W}_k \mathbf{d}_k e^{j2\frac{2\pi}{\mu K} kn} \quad (4)$$

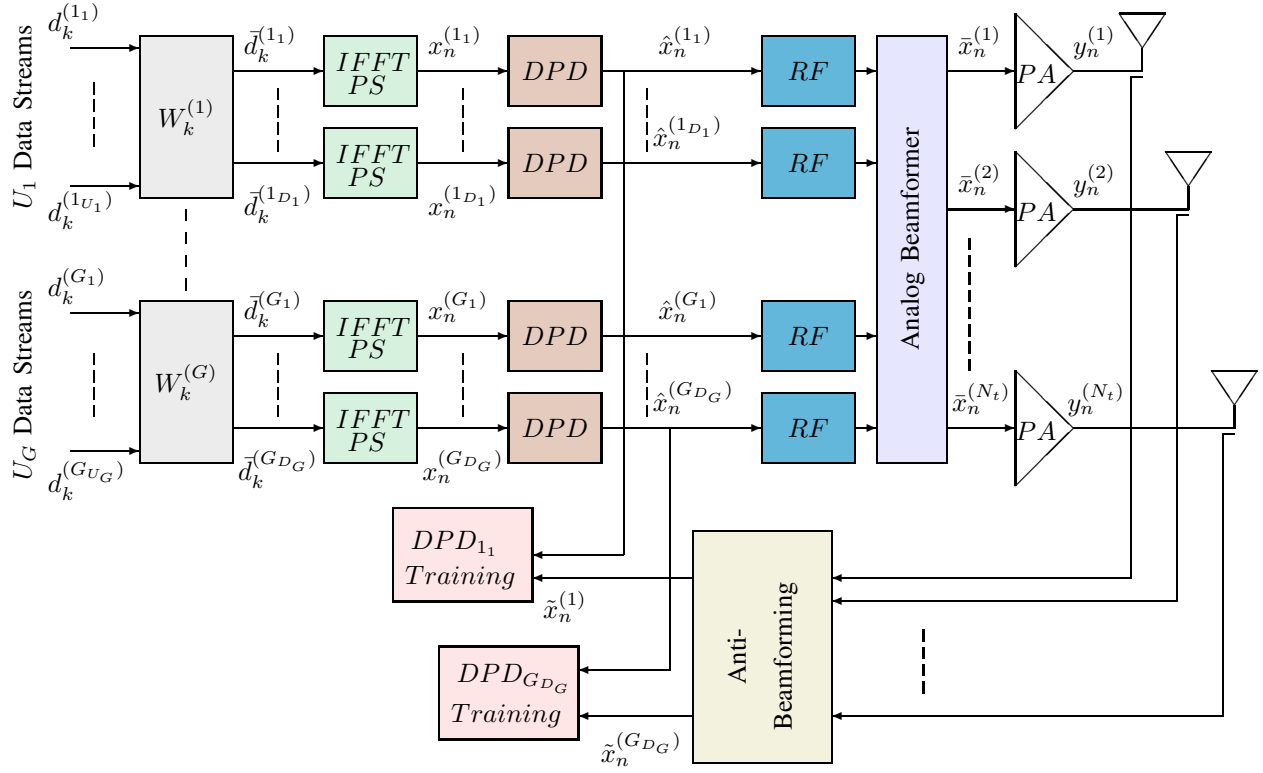


Fig. 1. Hybrid beamforming system architecture

where  $K$  is the number of QAM modulated active subcarriers,  $\mu$  is the oversampling factor,  $\mathbf{B} \in \mathbb{C}^{N_t \times D}$  is the analog beamformer matrix,  $\mathbf{W}_k \in \mathbb{C}^{D \times U}$  is the digital precoder matrix for  $k^{th}$  subcarrier,  $\mathbf{d}_k = [d_k^1, d_k^2, \dots, d_k^U]^T \in \mathbb{C}^{U \times 1}$  is *i.i.d.* distributed QAM modulated data symbols vector with autocorrelation,  $\mathbb{E}\{\mathbf{d}_k \mathbf{d}_{k-l}^H\} = \mathbf{I}\delta_l$ .

Due to impracticality of joint design of digital and analog beamformers, JSDM framework is adopted. In this framework, designs of beamformers are decoupled such that analog beamformer is formed based on second order statistics of the channel, while the digital precoder is designed by using reduced rank instantaneous effective channel. Digital precoder constitutes the first stage of the beamforming, which is used to isolate the intra-group users.

In this work, well-known zero-forcing precoding is employed, which is designed based on

the effective channel matrix of each group,  $\mathbf{H}_{eff,l}^{(g)} \triangleq [\mathbf{B}^{(g)}]^H \mathbf{H}_l^{(g)}$ , where  $\mathbf{B}^{(g)} \in \mathbb{C}^{N_t \times D_g}$  for  $g = 1, \dots, G$  is the sub-beamforming matrix for group  $g$  and  $\mathbf{H}_l^{(g)} = [\mathbf{h}_l^{(g_1)}, \dots, \mathbf{h}_l^{(g_{U_g})}]$  is the full dimension channel matrix for group  $g$ . In general, channel estimation is performed in reduced dimension; however, we assume that full rank channel is available at the BS since channel estimation is not in our scope. Overall analog beamforming matrix can be written in terms of the sub-beamformers for each group,  $\mathbf{B} = [\mathbf{B}^{(1)}, \mathbf{B}^{(2)}, \dots, \mathbf{B}^{(G)}]$ . For OFDM, frequency domain regularized zero-forcing precoder with regularization parameter  $\delta$  for a fixed analog beamformer is designed as,

$$\mathbf{W}_k^{(g)} \triangleq \mathbf{\Omega}_{eff,k}^{(g)} ([\mathbf{\Omega}_{eff,k}^{(g)}]^H \mathbf{\Omega}_{eff,k}^{(g)} + \delta \mathbf{I}_{U_g})^{-1}, \quad (5)$$

where  $\mathbf{\Omega}_{eff,k}^{(g)} = [\mathbf{B}^{(g)}]^H \mathbf{\Omega}_k^{(g)}$  is effective channel matrix in frequency domain and  $\mathbf{\Omega}_k^{(g)} = \sum_{l=0}^{\mu K-1} \mathbf{H}_l^{(g)} e^{-j2\pi l \frac{k}{\mu K}}$  is the frequency domain response for subcarrier  $k$  of group  $g$ .

Then, overall digital precoding matrix has the block diagonal form  $\mathbf{W}_k \triangleq bdiag\{\sqrt{c^{(g)}} \mathbf{W}_k^{(g)}\}_{g=1}^G$ , where  $c^{(g)}$  is the power scaling factor. It is determined such that operating points of PA's do not change over time. In the considered scenario, per group power constraint is adopted to obtain  $c^{(g)} = E_s / (GP^{(g)})$ , where  $E_s = \mathbb{E}\{|\mathbf{x}_n|^2\}$  is the total transmit power, and  $P^{(g)}$  is,

$$P^{(g)} \triangleq \frac{1}{K} \sum_{k=0}^{K-1} Tr\{\mathbf{B}^{(g)} \mathbf{W}_k^{(g)} [\mathbf{W}_k^{(g)}]^H [\mathbf{B}^{(g)}]^H\}. \quad (6)$$

Based on the power constraint expression in (6), it can be inferred that transmit power is kept constant for each channel realization.

### A. Design of Analog Beamformer

In hybrid structures, analog beamforming is applied to radiate the energy in the direction of the group of the intended user so that inter-group interference is suppressed. Analog beamformers can be classified into two groups based on the antenna array structure, namely "fully connected" and "partially connected" arrays. In fully connected array architecture shown in Fig. 2(a), each

antenna input is combination of all RF chains, while in partially connected array architecture shown in Fig. 2(b), each antenna input is dedicated to a single RF chain.

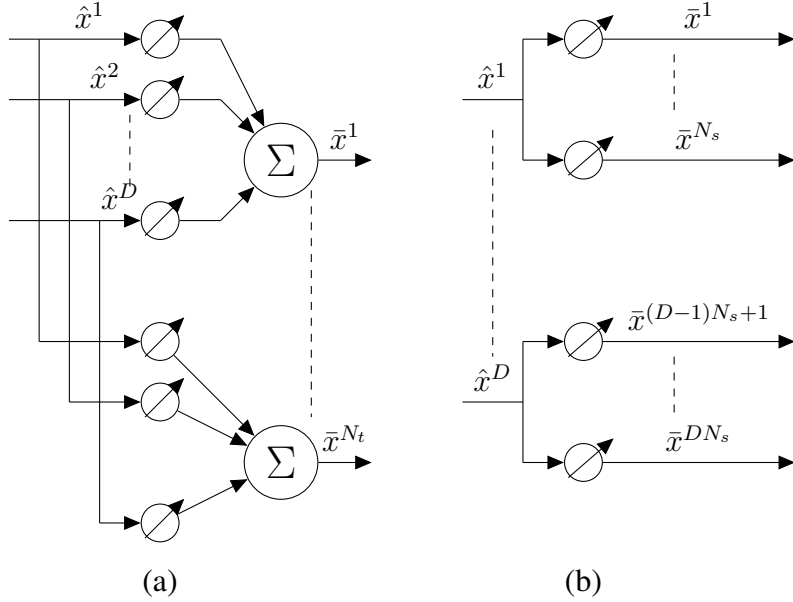


Fig. 2. Analog beamforming architectures (a) Fully connected (b) Partially connected architecture

1) *Fully Connected Array*: Angle only generalized eigen beamformer (AO-GEB), which is shown to be nearly optimal for several criteria in [11], is employed. Due to frequency domain equalization performed in OFDM modulation, CCM of the frequency domain impulse response should be used in design of analog beamformer. Since each MPC of a group is independent, we can show that  $\mathbb{E}\{\Omega_k^{(g)}[\Omega_k^{(g)}]^H\} = \sum_{l=0}^{\mu K-1} \mathbb{E}\{\mathbf{H}_l^{(g)} e^{-j2\pi l \frac{k}{\mu K}} [\mathbf{H}_l^{(g)}]^H e^{j2\pi l \frac{k}{\mu K}}\}$ ,  $\mathbb{E}\{\Omega_k^{(g)}[\Omega_k^{(g)}]^H\} = \sum_{l=0}^{L_g} \mathbf{R}_l^{(g)}$ . Hence, summation of CCM's of MPC's is used in GEB design. For each group, a sub-beamformer is formed as the first dominant  $D_g$  eigenvectors of the generalized eigenvalue problem,

$$\mathbf{B}^{(g)} = \text{eigs}(\mathbf{R}_{sum}^{(g)}, \mathbf{R}_{sum}, D_g) \quad (7)$$

where  $\mathbf{R}_{sum}^{(g)} = \sum_{l=0}^{L_g-1} \mathbf{R}_l^{(g)}$  and  $\mathbf{R}_{sum} = \sum_{g=1}^G \sum_{l=0}^{L_g-1} \mathbf{R}_l^{(g)} + N_o \mathbf{I}$ . In GEB, objective is to maximize the radiated power in the direction of the intended group while minimizing that of the

other groups. Despite the fact that fully connected array architecture performs close to optimal, it suffers from high complexity of implementation.

2) *Partially Connected Array*: Partially connected array architecture is a feasible structure to reduce the complexity of the array. For this architecture, analog beamforming matrix has the block diagonal form  $\mathbf{B} = bdiag(\mathbf{b}_1, \mathbf{b}_2, \dots, \mathbf{b}_D)$ , where  $\mathbf{b}_d = [b_d^1, b_d^2, \dots, b_d^{N_s}]^T \in \mathbb{C}^{N_s \times 1}$  is the sub-beamformer for the antenna array with  $N_s$  antennas of  $d^{th}$  RF chain. Phase only beamforming is a common approach, in which beamforming is applied via phase shifters where  $|b_d^m| = 1 \forall d, m$ . In this work, DFT beamformer is employed for phase only subarray.

In addition to phase only subarray, we propose a novel sub-beamformer design method for partially connected array architecture based on generalized eigen beamforming. Since phase only beamformers cannot suppress the inter-group interference sufficiently, we extend the GEB design, which is shown to be optimal for fully connected array architecture. In the proposed method, each sub-beamformer is obtained as the eigenvectors of the eigenvalue problem,

$$\mathbf{b}_{d_{gu}} = eigs(\mathbf{R}_{r,sum}^{(g_u)}, \mathbf{R}_{r,sum}, 1) \quad (8)$$

where  $\mathbf{R}_{r,sum}^{(g)} = \sum_{l=0}^{L_g-1} \mathbf{R}_{r,l}^{(g)}$  and  $\mathbf{R}_{r,sum} = \sum_{g=1}^G \sum_{u=1}^{U_g} \sum_{l=0}^{L_g-1} \mathbf{R}_{r,l}^{(g)}$ .  $\mathbf{R}_{r,l}^{(g)} \in \mathbb{C}^{N_s \times N_s}$  is the CCM in the reduced dimension of sub-array. In (8),  $D_g = U_g$  is assumed where each RF chain is assigned to a certain user; however, it can easily be extended to more general cases. CCM in reduced dimension is obtained with an array of size  $N_s$  placed at the origin. This yields a phase offset in the effective channel matrix; however, digital precoding makes necessary phase correction in digital domain. Besides, this approach assumes that users in a group are distinguishable but close in angular domain so that they can be grouped together. Therefore, individual CCM's can be obtained for each user in a group.

#### IV. COMPENSATION METHODS FOR PA NONLINEARITIES

Two methods will be presented in order to compensate the effects of PA nonlinearities. First method is the well known DPD, which aims to predict the distortion caused by the nonlinear

PA and predistorts the signal such that overall transmitted signal has the desired form. The other compensation method is based on Bussgang decomposition for each subcarrier at the user terminal. This method corresponds to frequency domain equalization for the linear channel formed by the memory of PA which is not considered in design of the digital precoder.

### A. DPD for Hybrid Beamforming Architecture

In this section, we present the DPD design framework for hybrid beamforming architecture, which employs anti-beamforming in order to reduce the dimension of the observation space to the number of RF chains. In literature, there are several methods that address anti-beamforming, which is implemented by reverse phase shifting; however, these works consider phase only subarray networks as analog beamformer. However, this approach is not valid for the proposed GEB since beamforming gains are not unity in general and required anti-beamforming is a more complex task.

Consider the transmitted signal from antenna array,  $\mathbf{y}_n = [y_n^{(1)}, y_n^{(2)}, \dots, y_n^{(N_t)}]^T$ , where  $y_n^{(m)} = \Psi(\bar{x}_n^{(m)})$  and  $\Psi(\cdot)$  represents, PA nonlinearity defined in (3). Thus, transmitted signal from the antenna array can be expressed as,

$$\mathbf{y}_n = \sum_{\varpi=-\Pi+1}^{\Pi-1} \sum_{v=0}^{\Upsilon-1} \alpha_{\varpi,v} \bar{\mathbf{x}}_{n-\varpi} \odot |\bar{\mathbf{x}}_{n-\varpi}|^{2v} \quad (9)$$

where  $\bar{\mathbf{x}}_n$  is the analog beamformed signal. By expressing  $\bar{\mathbf{x}}_n$  in terms of digital predistorted signal, one can obtain,

$$\mathbf{y}_n = \sum_{\varpi=-\Pi+1}^{\Pi-1} \sum_{v=0}^{\Upsilon-1} \alpha_{\varpi,v} [(\mathbf{B} \hat{\mathbf{x}}_{n-\varpi}) \odot |\mathbf{B} \hat{\mathbf{x}}_{n-\varpi}|^{2v}], \quad (10)$$

where  $\odot$  denotes the Hadamard product and for simplicity all PA's are assumed to be identical. In the proposed architecture,  $N_t \times 1$  observation vector,  $\mathbf{y}_n$ , is used to design  $D$  DPD units. Hence, it is necessary to project the  $N_t \times 1$  observations to the reduced dimension of  $D \times 1$ . For this purpose, consider the beamformed signal,  $\bar{\mathbf{x}}_u = \mathbf{B} \hat{\mathbf{x}}_n$ , where it can be written in terms of sub-beamformers  $\bar{\mathbf{x}}_u = \mathbf{B}^{(1)} \hat{\mathbf{x}}^{(1)} + \mathbf{B}^{(2)} \hat{\mathbf{x}}^{(2)} + \dots + \mathbf{B}^{(G)} \hat{\mathbf{x}}^{(G)}$ .

In this study, anti-beamforming is performed by projecting the observation vector onto the sub-spaces, which are spanned by the sub-beamformers. DPD's for each group are designed based on the observation vector projected onto corresponding sub-beamformer space. Proposed approach employs pseudo-inverses of the sub-beamformers for the projection via anti-beamforming matrix,  $\mathbf{B}_{ab} = [([\mathbf{B}^{(1)}]^\#)^T, ([\mathbf{B}^{(2)}]^\#)^T, \dots, ([\mathbf{B}^{(G)}]^\#)^T]^T$ , where  $[\mathbf{B}^{(g)}]^\#$  is the pseudo inverse matrix of  $\mathbf{B}^{(g)}$ . Then the projected observation vector becomes,

$$\begin{aligned} \tilde{\mathbf{x}}_n = & \alpha_{0,0} \mathbf{B}_{ab} \mathbf{B} \hat{\mathbf{x}}_n + \sum_{v=1}^{\Upsilon-1} \alpha_{0,v} \mathbf{B}_{ab} [(\mathbf{B} \hat{\mathbf{x}}_n) \odot |\mathbf{B} \hat{\mathbf{x}}_n|^{2v}] + \\ & \sum_{\substack{\varpi=-\Pi+1, \\ \varpi \neq 0}}^{\Pi-1} \sum_{v=0}^{\Upsilon-1} \alpha_{\varpi,v} \mathbf{B}_{ab} [(\mathbf{B} \hat{\mathbf{x}}_{n-\varpi}) \odot |\mathbf{B} \hat{\mathbf{x}}_{n-\varpi}|^{2v}], \end{aligned} \quad (11)$$

where  $\mathbf{B}_{ab} \mathbf{B} \approx \mathbf{I}_D$  since sub-beamformers are designed to be orthogonal to each other. Second and third terms in (11) correspond to remaining interference, which depends on the distorted signals on all RF chains due to nonlinearity. Power of the interference term limits the performance of the DPD. After obtaining the projected values, one can form the error signal as  $\mathbf{e}_n = \hat{\mathbf{x}}_n - \tilde{\mathbf{x}}_n$ . Error signal,  $\mathbf{e}_n$ , can be used to design the polynomial DPD by using indirect learning architecture (ILA) for  $d^{th}$  RF branch,

$$\hat{x}_n^d = \sum_{\varpi=-\Pi'+1}^{\Pi'-1} \sum_{v=0}^{\Upsilon'-1} w_{\varpi,v}^d x_{n-\varpi}^d |x_{n-\varpi}^d|^{2v} \quad (12)$$

where,  $w_{\varpi,v}^d$  are the DPD coefficients and they can be found by using least squares (LS) method proposed in [31] as,

$$\mathbf{w}_b^d = \mathbf{w}_{b-1}^d + \beta (\mathbf{X}_d^H \mathbf{X}_d)^{-1} \mathbf{X}_d^H \mathbf{e}^d \quad (13)$$

where  $\mathbf{w}_b^d$  is the DPD coefficient vector calculated at  $b^{th}$  block,  $\mathbf{X}_d$  is the observation matrix whose elements are  $\tilde{x}_{n-\varpi}^d |\tilde{x}_{n-\varpi}^d|^v$ ,  $\mathbf{e}^d = [e_n^d e_{n-1}^d \dots e_{n-L+1}^d]^T$  is the error vector for  $d^{th}$  RF branch,  $L$  is the number of samples and  $\beta$  is the step-size for the adaptation. It should be noted that DPD for each RF chain is designed individually due to multiplexing caused by analog beamformer even if all PA's are identical.

### B. Post Equalization at User Terminal

A linear post equalizer is proposed in order to compensate the memory effects of PA's on the transmit chain as a simpler alternative to DPD. At BS, a pre-equalization is applied by means of digital precoding based on CSI acquired by uplink training. However, there is an undesired linear channel due to memory of PA's, which is ignored during the design of digital precoder. Therefore, an equalization procedure is necessary at the receiver side. In this work, Bussgang decomposition is applied for each sub-carrier at the receiver. Received signal at  $g_u^{th}$  user after FFT operation for each subcarrier,  $r_k^{(g_u)}$ , can be expressed as,

$$r_k^{(g_u)} = \alpha_k^{(g_u)} d_k^{(g_u)} + \eta_k^{(g_u)}, \quad (14)$$

where  $\alpha_k^{(g_u)}$  is the frequency domain Bussgang coefficient and  $\eta_k^{(g_u)}$  is the distortion term. Since Bussgang coefficient is defined for each subcarrier, it can be interpreted as the frequency domain channel for the corresponding subcarrier as in [21] and it is obtained as,

$$\alpha_k^{(g_u)} = \frac{\mathbb{E}\{r_k^{(g_u)}[d_k^{(g_u)}]^*\}}{\mathbb{E}\{|d_k^{(g_u)}|^2\}}. \quad (15)$$

By using scalar channel coefficient given in (15), symbol estimate is obtained as,

$$\hat{d}_k^{(g_u)} = \frac{r_k^{(g_u)}}{\alpha_k^{(g_u)}}. \quad (16)$$

## V. PERFORMANCE MEASURES

In this study, performance of the proposed DPD structure is evaluated via several performance criteria. Firstly, power spectral density (PSD) of the received signal at different locations are evaluated. Beampatterns for the in-band and out-of-band radiation are presented in order to understand the effect of hybrid beamforming on the radiation pattern for different architectures. Then, by using GMI metric, AIR for the proposed architecture is obtained via the mismatch capacity framework. Lastly, a comprehensive analysis on BER performance is pursued by deriving signal to interference plus noise ratio (SINR) expressions for different array architectures.

### A. Radiation Patterns

Radiation pattern is evaluated by investigating the PSD of the received signal at different angles. For this purpose, channel for any direction,  $(\theta)$ , is approximated as the steering vector,  $\mathbf{a}^H(\theta)$ , pointing that direction. Then PSD,  $S_r^\theta(f) = \sum_{t=-\infty}^{\infty} R_t^\theta e^{-j2\pi f t}$ , is obtained by taking the Fourier Transform of the autocorrelation function,  $R_t^\theta = \mathbb{E}[r_n^\theta(r_{n-t}^\theta)^H]$ , of the artificially generated received signal,  $r_n^\theta = \mathbf{a}^H(\theta)\mathbf{y}_n$ . Using  $S_r^\theta(f)$ , in-band and out-of-band radiation powers are calculated as,

$$P_{ib}(\theta) = \int_{-B/2}^{B/2} S_r^\theta(f) df, \quad (17)$$

$$P_{ob}(\theta) = \max\left\{\int_{-3B/2}^{-B/2} S_r^\theta(f) df, \int_{B/2}^{3B/2} S_r^\theta(f) df\right\} \quad (18)$$

where  $P_{ib}(\theta)$  and  $P_{ob}(\theta)$  are the in-band and out-of-band radiation patterns in  $\theta$  direction respectively.

### B. Generalized Mutual Information (GMI)

In this section, mismatch GMI concept, which is used to obtain a lower bound for the achievable rate for the channels with unknown probability density function (PDF), is presented. In the considered problem, PA can be considered as a nonlinear channel, whose PDF is not known. For this purpose, GMI metric, presented in [26], is adopted to obtain AIR value. In [26], GMI expression is given as,

$$C = \log_2 M - E_{d,r} \left[ \log_2 \left( \frac{\sum_{d' \in A_d} p(r|d')}{p(r|d)} \right) \right], \quad (19)$$

where  $A_d$  is QAM symbol alphabet,  $M$  is the modulation order.  $p(r|d)$  is the conditional PDF of the decoded signal  $r$  given that symbol  $d$  is sent. In AWGN channel case,  $p(r|d)$  has the Gaussian form; however, due to the nonlinearity caused by PA, Gaussian PDF is not valid. Thus, in this study, we employ an approximation of this PDF so that mismatch capacity introduced in [27]–[29], can be calculated. A lower bound on the mismatch capacity is expressed as,

$$C_M = \log_2 M - E_{d,r} \left[ \log_2 \left( \frac{\sum_{d' \in A_d} \tilde{p}(r|d')}{\tilde{p}(r|d)} \right) \right], \quad (20)$$

where  $\tilde{p}(r|d')$  is the mismatched PDF.

1) *Mismatch PDF at the receiver side*: In order to write the mismatched PDF, one should relate the decoded symbol to actual symbol. For this purpose, we use well-known Bussgang theorem in order to decompose linear undistorted and the nonlinear distorted terms in frequency domain as,  $r_k = \hat{\alpha}_k d_k + \eta_k$ , where  $\hat{\alpha}_k$  is the Bussgang coefficient per subcarrier and  $\eta_k$  is the distortion term with power  $\sigma_\eta^2 = \mathbb{E}[\eta_k^H \eta_k]$  and it is orthogonal to linear signal term,  $\mathbb{E}[d_k^H \eta_k] = 0$ . Bussgang coefficient,  $\hat{\alpha}_k$  can be found by Wiener filtering,

$$\hat{\alpha}_k = \frac{\mathbb{E}[d_k^H r_k]}{\mathbb{E}[d_k^H d_k]}. \quad (21)$$

Having defined Bussgang decomposition, mismatched PDF can be expressed in terms of Bussgang coefficient and the distortion power,

$$\tilde{p}(r|d') = \frac{1}{\pi \sigma_\mu^2} \exp \left( -\frac{|r_k - \hat{\alpha}_k d_k|^2}{\sigma_{\eta,k}^2} \right). \quad (22)$$

Mismtached PDF defiend in (22) is valid for systems utilizing post equalization at UT's. Moreover, mismatch PDF can also be written for the systems without any receiver side equalization as,

$$\tilde{p}(r|d') = \frac{1}{\pi \sigma_\eta^2} \exp \left( -\frac{|r_k - \hat{\alpha} d_k|^2}{\sigma_{\eta,k}^2} \right), \quad (23)$$

where  $\hat{\alpha}$  is the single phase and amplitude correction term defined as,

$$\hat{\alpha} = \frac{\sum_{k=0}^{K-1} r_k d_k^*}{\sum_{k=0}^{K-1} |d_k|^2}. \quad (24)$$

Mismtached PDF defiend in (22) can also be used for the systems employing DPD at the transmitter since DPD also compensates the memory effects of the PA's. Hence, equalization at UT is not necessary. Consequently, achievable capacity bound can be obtained by inserting mismatch PDF expressions (22) and (23) into (20). In (21) and (24), Bussgang coefficients are considered as independent of constellation point due to multiplexing of different symbols in precoders.

### C. Bit-Error-Rate Analysis

A comprehensive analysis on BER performances of the different array structures is carried out to obtain an analytical approximation for probability of bit error. A general Bussgang decomposition is developed for multidimensional signal domain in which Bussgang coefficient has a matrix form rather than a single scalar due to correlation between signals on different antennas. Based on proposed Bussgang decomposition, SINR expression is obtained and BER is expressed as a function of SINR. For this purpose, nonlinear channel is modelled in frequency domain for different array architectures. For the rest of the analysis, digitally precoded,  $\mathbf{x}_k^f$ , and analog beamformed,  $\mathbf{y}_k^f$ , signals should be defined in frequency domain,

$$\mathbf{x}_k^f = \frac{1}{\sqrt{\mu K}} \sum_{n=0}^{\mu K-1} \mathbf{x}_n e^{j \frac{2\pi}{\mu K} nk}, \quad (25)$$

$$\mathbf{y}_k^f = \frac{1}{\sqrt{\mu K}} \sum_{n=0}^{\mu K-1} \mathbf{y}_n e^{j \frac{2\pi}{\mu K} nk}. \quad (26)$$

*1) Fully Connected Array:* Conventional approaches consider Bussgang decomposition on PA basis; however, in this work, we propose a new decomposition scheme where analog beamformer is also taken into account together with PA's. Consequently, a spatio-temporal Bussgang decomposition is performed which is a mapping from reduced dimensional digital precoded signal vector,  $\mathbf{x}_k^f$ , to full dimensional transmitted signal,  $\mathbf{y}_k^f$ . Motivated by this approach, Bussgang decomposition is applied in matrix-vector form as,

$$\mathbf{y}_k^f = \mathbf{A}_k \mathbf{x}_k^f + \eta_k \quad (27)$$

where  $\mathbf{A}_k \in \mathbb{C}^{N \times D}$  can be considered as the linearized analog beamforming matrix after nonlinear amplification and  $\eta_k$  is the nonlinear distortion vector for  $k = 0, 1, \dots, \mu K$ . In addition,  $\mathbf{A}_k$  can be written in terms of sub-beamformers as  $\mathbf{A}_k = [\mathbf{A}_k^{(1)}, \mathbf{A}_k^{(2)}, \dots, \mathbf{A}_k^{(G)}]$ , which will be used later while defining different interference terms.  $\mathbf{A}_k$  can be obtained as the generalization of the scalar Bussgang decomposition to matrix form,

$$\mathbf{A}_k = \mathbb{E} \left[ \mathbf{y}_k^f (\mathbf{x}_k^f)^H \right] \left( \mathbb{E} \left[ \mathbf{x}_k^f (\mathbf{x}_k^f)^H \right] \right)^{-1}. \quad (28)$$

One should note that if all the PA's were linear then Bussgang matrix would be analog beamformer matrix,  $\mathbf{A}_k = \mathbf{B}$ . Due to correlation between different antennas, distortion terms are also correlated. Hence autocorrelation matrix for the distortion vector,  $\mathbf{R}_\eta^k$ , is important for the rest of the analysis,

$$\mathbf{R}_\eta^k = \mathbb{E} \left[ (\mathbf{y}_k^f - \mathbf{A}_k \mathbf{x}_k^f) (\mathbf{y}_k^f - \mathbf{A}_k \mathbf{x}_k^f)^H \right]. \quad (29)$$

2) *Partially Connected Array*: In partially connected array structure, Bussgang coefficients are defined as vectors for each sub-array since in this structure each sub-array is driven by a single RF chain. Therefore, transmitted signal for a sub-array can be expressed as,

$$\mathbf{y}_k^{(g_u),f} = \mathbf{a}_k^{(g_u)} x_k^{(g_u),f} + \eta_k, \quad (30)$$

then linearized sub-beamformer can be expressed as,

$$\mathbf{A}_k^{(g)} = \mathbf{e}_{G,g} \otimes \sum_{u=1}^{U_g} \mathbf{E}_{U_g,u} \otimes \mathbf{a}_k^{(g_u)}, \quad (31)$$

where  $\mathbf{e}_{G,g}$  is the  $G$  dimensional elementary vector whose elements are 0 except  $g^{th}$  entry which is 1 and  $\mathbf{E}_{G,g}$  is the  $U_g$  dimensional elementary matrix whose elements are 0 except  $u^{th}$  diagonal entry which is 1. For simplicity in (31), it assumed that number of RF chains are the same as number of users and each RF chain is dedicated to a single user.

By using signal model given in (30), one can define Bussgang decomposition for partially connected array as,

$$\mathbf{a}_k^{(g_u)} = \frac{\mathbb{E} \left[ \mathbf{y}_k^f (\mathbf{x}_k^f)^* \right]}{\mathbb{E} [|x_k^f|^2]}. \quad (32)$$

Distortion covariance matrix,  $\mathbf{R}_\eta^k = bdiag\{\mathbf{R}_\eta^{(d),k}\}_{d=1}^D$ , has the block diagonal form since only the distortion terms in the same subarray are correlated, where  $\mathbf{R}_\eta^{(d),k} = \mathbb{E} \left[ \eta_k^{(d)} (\eta_k^{(d)})^H \right]$  is the autocorrelation matrix of the distortion terms of  $d^{th}$  subarray.

3) *Fully Digital Beamforming*: For fully digital beamforming architectures, the standard Bussgang decomposition can be applied for each antenna in the system,

$$y_k^{m,f} = a_k^m x_k^{m,f} + \eta_k^m, \quad (33)$$

where  $a_k^m$  is the Bussgang coefficient for  $m^{th}$  antenna defined as in (21) contrary to single Bussgang coefficient defined for each antenna for fully digital systems in literature [19], [20], [22].

Having introduced the Bussgang decomposition in multidimensional domain, equivalent received signal model at UT's can be obtained. Firstly, consider the input to nonlinear channel,

$$\mathbf{x}_n = \sum_{k=0}^{\mu K-1} \frac{1}{\mu K} bdiag\{\sqrt{c^{(g)}} \mathbf{W}_k^{(g)}\}_{g=1}^G \mathbf{d}_k e^{j \frac{2\pi}{\mu K} kn}, \quad (34)$$

and also define the channel of the user  $g_u$  in frequency domain as the  $g_u^{th}$  column of the channel matrix in frequency domain,  $\omega_k^{(g_u)} \triangleq \mathbf{\Omega}_k^{(g)}[:, u]$  and digital precoder for the same user is  $\mathbf{w}_k^{(g_u)} \triangleq \mathbf{W}_k^{(g)}[:, u]$  for  $u = 1, \dots, U_g$ . After taking DFT at UT for user  $g_u$ , one can express the received signal in frequency domain as,

$$\begin{aligned} r_k^{(g_u)} &= [\omega_k^{(g_u)}]^H \mathbf{y}_k^f + \nu_k^{(g_u)}, \quad k = 0, 1, \dots, \mu K - 1 \\ &= [\omega_k^{(g_u)}]^H (\mathbf{A}_k \mathbf{x}_k^f + \eta_k) + \nu_k^{(g_u)}, \\ &= [\omega_k^{(g_u)}]^H \left[ \sum_{g=1}^G \sqrt{c^{(g)}} \mathbf{A}_k^{(g)} \mathbf{W}_k^{(g)} \mathbf{d}_k^{(g)} + \eta_k \right] + \nu_k^{(g_u)} \end{aligned} \quad (35)$$

Last term in (35) is decomposed such that different interference terms can be measured separately,

$$\begin{aligned} r_k^{(g_u)} &= \underbrace{\sqrt{c^{(g)}} [\omega_k^{(g_u)}]^H \mathbf{A}_k^{(g)} \mathbf{w}_k^{(g_u)} d_k^{(g_u)}}_{\text{desired signal term}} + \underbrace{\sqrt{c^{(g)}} \sum_{\substack{u'=1 \\ u \neq u}}^{U_g} [\omega_k^{(g_u)}]^H \mathbf{A}_k^{(g)} \mathbf{w}_k^{(g_u')} d_k^{(g_u')}}_{\text{intra-group interference}} \\ &\quad + \underbrace{\sum_{\substack{g'=1 \\ g \neq g'}}^G \sqrt{c^{(g')}} [\omega_k^{(g_u)}]^H \mathbf{A}_k^{(g')} \mathbf{W}_k^{(g')} \mathbf{d}_k^{(g')}}_{\text{inter-group interference}} + \underbrace{[\omega_k^{(g_u)}]^H \eta_k}_{\text{nonlinear distortion}} + \underbrace{\nu_k^{(g_u)}}_{\text{AWGN}}. \end{aligned} \quad (36)$$

By using (36), instantaneous SINR at the receiver is obtained as,

$$SINR_k^{(g_u)} = \frac{c^{(g)} |[\omega_k^{(g_u)}]^H \mathbf{A}_k^{(g)} \mathbf{w}_k^{(g_u)}|^2}{\sigma_{I,N,k}^2} \quad (37)$$

where  $\sigma_{I,N,k}^2$  is the total interference-plus-noise power expressed as,

$$\begin{aligned} \sigma_{I,N,k}^2 = c^{(g)} \sum_{\substack{u'=1 \\ u \neq u}}^{U_g} |[\omega_k^{(g_u)}]^H \mathbf{A}_k^{(g)} \mathbf{w}_k^{(g_u)}|^2 + \sum_{\substack{g'=1 \\ g \neq g'}}^G c^{(g')} [\omega_k^{(g_u)}]^H \mathbf{A}_k^{(g')} \mathbf{W}_k^{(g')} [\mathbf{W}_k^{(g')}]^H [\mathbf{A}_k^{(g')}]^H \omega_k^{(g_u)} \\ + [\omega_k^{(g_u)}]^H \mathbf{R}_\eta^k \omega_k^{(g_u)} + N_o. \end{aligned} \quad (38)$$

By using SINR expression given in (37), the average BER can be obtained as,

$$P_b = \frac{1}{U} \sum_{g=1}^G \sum_{u=1}^{U_g} \frac{4}{\log_2(M)} \left(1 - \frac{1}{\sqrt{M}}\right) \mathbb{E}_{\omega_k^{(g_u)}} \left[ Q \left( \sqrt{\frac{3}{M-1}} SINR_k^{(g_u)} \right) \right], \quad (39)$$

where  $Q(x) = \frac{1}{\sqrt{2\pi}} \int_x^\infty e^{(-t^2/2)} dt$ .

## VI. NUMERICAL RESULTS

Numerical results are presented in order to compare different beamforming architectures under PA nonlinearities in terms of their radiation patterns, achievable information rates and bit error rates. Furthermore, analytical expression of BER is verified by the Monte Carlo trials. In this study, all PA's are assumed to be identical but their operating points depend on the gain of analog beamforming. In the simulations, PA model for  $\sim 2$  GHz commercially available GaAs PA, which is presented in [32], is used.  $N_t = 96$  antennas having ULA geometry is placed at BS. There are  $D = 6$  RF chains so each sub-array consists  $N_s = 16$  antennas in partially connected array structure. In the considered scenario, there are  $G = 3$  groups, each group having 2 users and also there is a victim user who is served by another BS. The user and victim distribution is summarized in Table I. It is assumed that line-of-sight (LOS) component always exist for each angular sector with Rician factor  $K = 10$  dB. Also, the power of LOS component is 3 dB larger than the power of second MPC component (MPC). In generated OFDM signal, number of subcarriers and IFFT size are  $K = 550$  and  $\mu K = 4096$ , respectively, and cyclic prefix length is selected as  $N_{cp} = 20$ .

TABLE I  
SCENARIO

Group	# of MPC's	1 <sup>st</sup> MPC Angular Sector	2 <sup>nd</sup> MPC Angular Sector
1	2	[-22°, -28°]	[-17°, -11°]
2	2	[-4°, 2°]	[14°, 8.5°]
3	1	[27°, 21°]	-
Victim	1	[-36°, -39°]	-

### A. Power Spectral Density and Radiation Pattern Analysis

Power spectra and radiation patterns of the array structures are obtained in order to assess the severity of the unwanted power emissions in both frequency and spatial domains. In Fig. 3, average PSD's of signals received by the users are shown. It is observed that OOB is a significant problem for all beamforming architectures. However, classical DPD is shown to be a feasible solution for investigated array structures except fully connected array since power leakage to adjacent channel is suppressed notably. In fully connected structure, however, classical DPD does not provide any improvement when OOB radiation is considered. It can be observed that DPD provides the best performance for fully digital system since there is a single DPD unit dedicated to each antenna element.

Furthermore, we investigate spatial distribution of in-band and out-of-band power emissions for different array architectures. Radiation pattern is a substantial metric since it demonstrates the power leakage to neighbourhood frequency bands for different directions. Power angular spectrum for in-band radiation in Fig. 4, shows that nonlinear effects do not distort the beam-pattern of the antenna array. Another important conclusion that can be drawn from in-band radiation pattern is abouth the null level of the array with GEB. Due to nonlinear distortion, null level of the array gets higher, which degrades the inter-group interference suppression capability.

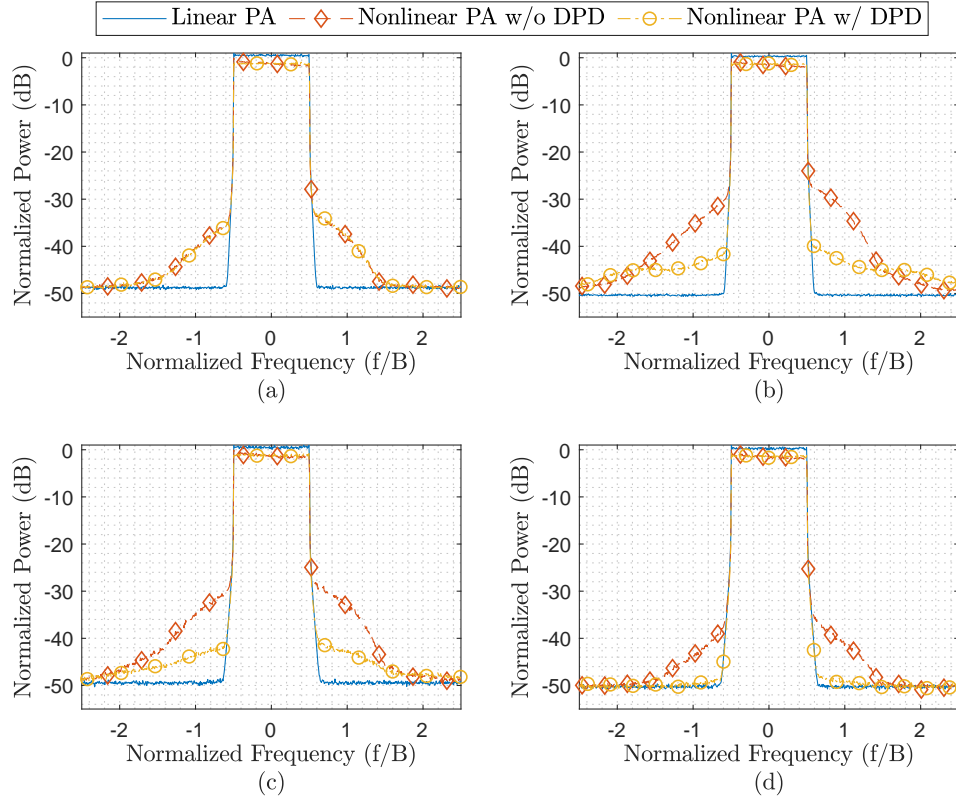


Fig. 3. Normalized average power spectral density of intended users for different array architectures equipped with nonlinear PA's (a) fully connected (b) partially connected with GEB (c) partially connected with phase only subarray (d) fully digital beamforming.

However, despite the higher null level, a significant amount of suppression is still achieved compared to phase only subarray.

In Fig. 5, power angular spectrum for out-of-band radiation is shown. Out-of-band band power is also concentrated in the served user directions. Similar to PSD analysis, DPD does not provide improvement in the OOB radiation in any direction as can be seen in Fig. 5(a), for fully connected architecture. On the other hand, employing DPD at the transmitter significantly decreases OOB emission for partially connected array and fully digital precoding architectures. However, it is also observed that radiated power in fully connected architecture is not much higher than that of

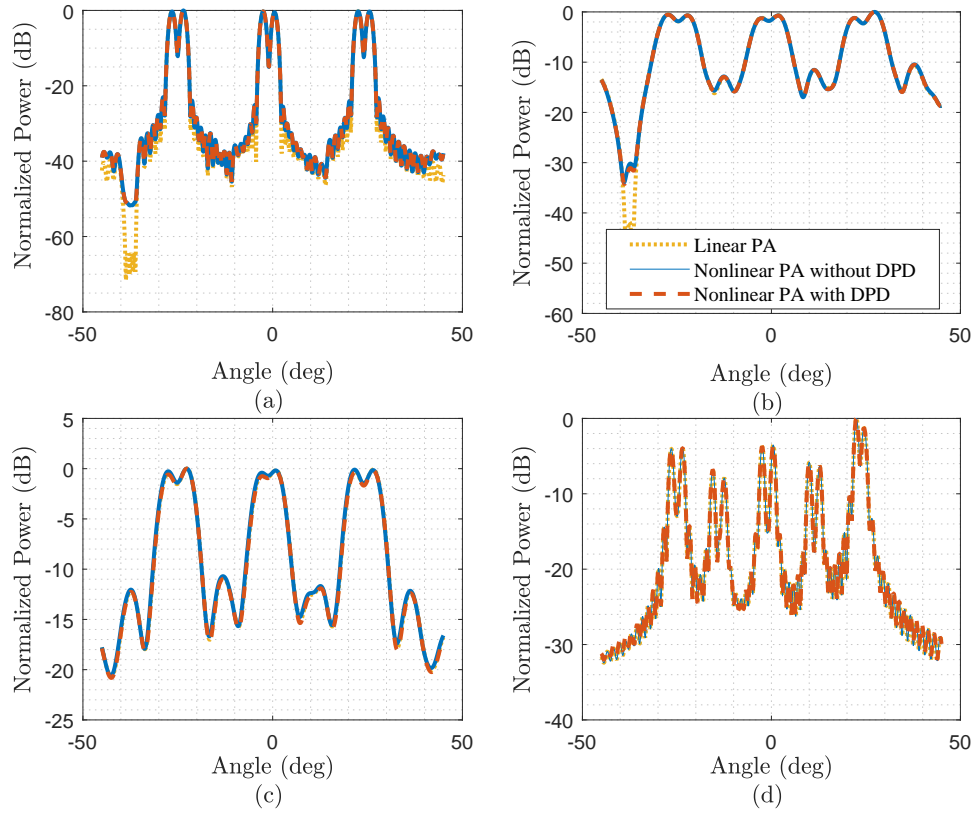


Fig. 4. In-band power radiation pattern from BS for the interval of -50 and 50 degrees for different array architectures (a) fully connected (b) partially connected with GEB (c) partially connected with phase only subarray (d) fully digital beamforming. Maximum in-band power is scaled to be 0 dB.

partially connected arrays with DPD since its multiplexing gain is larger than the multiplexing gain of partially connected array. The reason is that in fully connected structure all,  $N_t = 96$ , are used to transmit the signal to a single user. On the other hand, only a sub-array of size,  $N_s = 16$ , is dedicated for a single user in partially connected systems. Also, at the UT, desired signal term is combined coherently, while distortion term is combined non-coherently, consequently, effects of the nonlinear distortion is averaged out in fully connected and partially connected architectures compared to partially connected architecture.

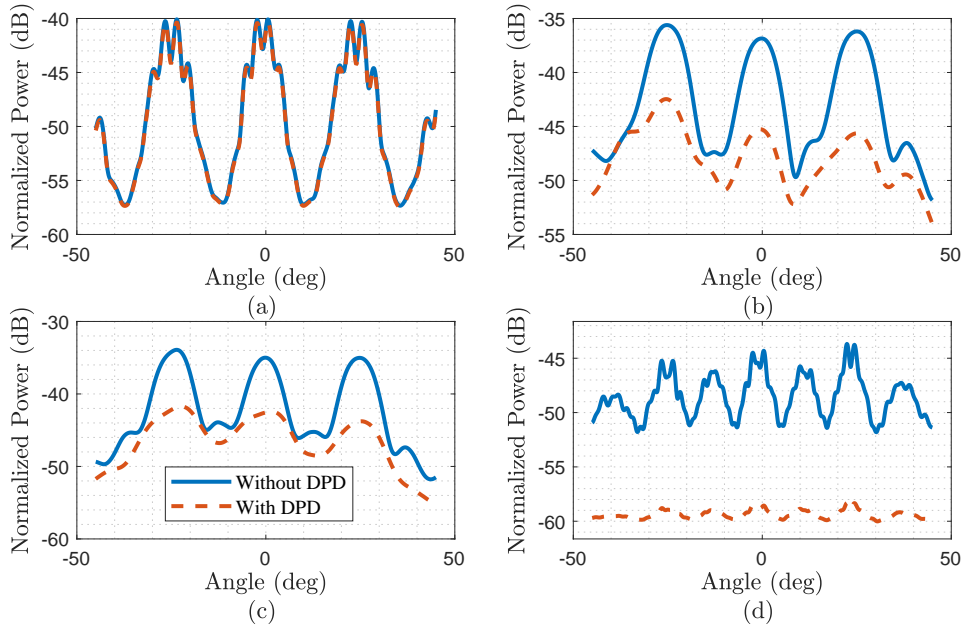


Fig. 5. Out-of-band power radiation pattern from BS for the interval of -50 and 50 degrees for different array architectures (a) fully connected (b) partially connected with GEB (c) partially connected with phase only subarray (d) fully digital beamforming. Maximum in-band power is scaled to be 0 dB.

### B. GMI Analysis

Having investigated the spatial radiation of the transmitted power, we can now compare the AIR performances of the different beamforming architectures with different processing techniques. For this purpose, GMI analysis is carried out for these structures. Capacity curves are obtained for a constant transmitted power,  $E_s$  and  $E_s/N_o$ , which is the received signal to noise ratio (SNR) per-subcarrier, is adjusted by modifying the receiver noise power. Firstly, from Fig. 6, it can be inferred that array structures has vital impact on the capacity of the system. Phase only subarray cannot achieve the maximum AIR regardless of the noise level and nonlinear distortion. Even for linear PA, capacity of this architecture is limited due to inter-group interference. However, the other structures can successfully suppress both inter-group and intra-

group interferences, which make them superior compared to phase only beamforming. Apart from array structure, nonlinear distortion introduced by PA has notable effect on the performance since systems with linear PA's can reach higher spectral efficiency for the same noise level compared to systems with nonlinear PA's, until it is limited by the constellation order.

Both systems with fully connected and fully digital array architectures can achieve maximum capacity by employing either equalization at UT or DPD, and these methods exhibit close performances for both architectures. The reason is that nonlinear distortion is already suppressed by the diversity; therefore, linear processing is sufficient. On the other hand, multiplexing gain cannot be fully exploited by partially connected systems due to decrease in the effective antenna per user, which decreases the multiplexing gain. Therefore, maximum capacity cannot be reached by employing linear receiver processing in GEB subarray whereas it is achieved by conventional DPD since it suppresses nonlinear distortion as well. Consequently, classical DPD technique is proven to be a feasible solution. Lastly, one can see that the systems, which do not employ any processing, suffer from significant performance degradation for all array architectures.

### *C. BER Analysis*

In this section, analysis on uncoded BER performances of the arrays structures are evaluated. Derived analytical BER expression is verified with numerical Monte Carlo simulations for 64 and 256 QAM constellations. Fig. 7 presents theoretical and numerical BER curves. It can be seen that analytical BER curves are in compliance with the numerical results. However, there is a divergence in case of fully digital beamforming with 256 QAM, which is acceptable since BER approximation for a higher order modulation is employed and which may not be exact but it sets a bound for BER. Also note that BER results for the system, which does not employ any processing, is not considered in BER analysis due to its poor AIR performance.

Firstly, it can be observed that phase only subarray exhibits significantly higher error floor compared to other architectures. For fully digital beamforming; on the other hand, both DPD and

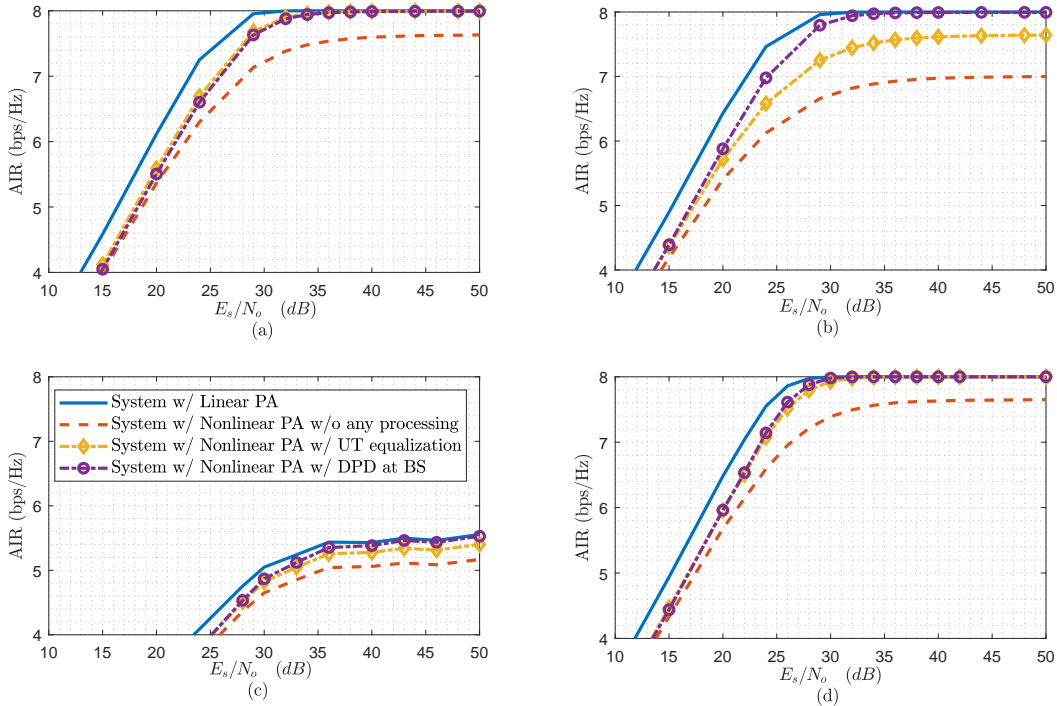


Fig. 6. Average mismatched capacity of users for 256 QAM for different array architectures (a) fully connected (b) partially connected with GEB (c) partially connected with phase only subarray (d) fully digital beamforming.

equalization methods perform close to linear PA in case of 64 QAM; however, post-equalization method suffers from a performance degradation for 256 QAM.

Similar to fully digital structure, both DPD and equalization methods also perform close to linear PA for 64 QAM for fully connected structure. However, there exists an error floor for the systems with nonlinear PA for 256 QAM. From these results, one can conclude that classical DPD does not provide any improvement due to nature of fully connected structure. In fully connected structure, each PA is connected to all RF chains; however, each DPD is designed based on a single RF chain. Therefore, DPD's cannot compensate the nonlinear distortion, they only compensate the memory effects of PA's. This can be also verified by the simulations since equalization at UT and DPD at BS performs very closely.

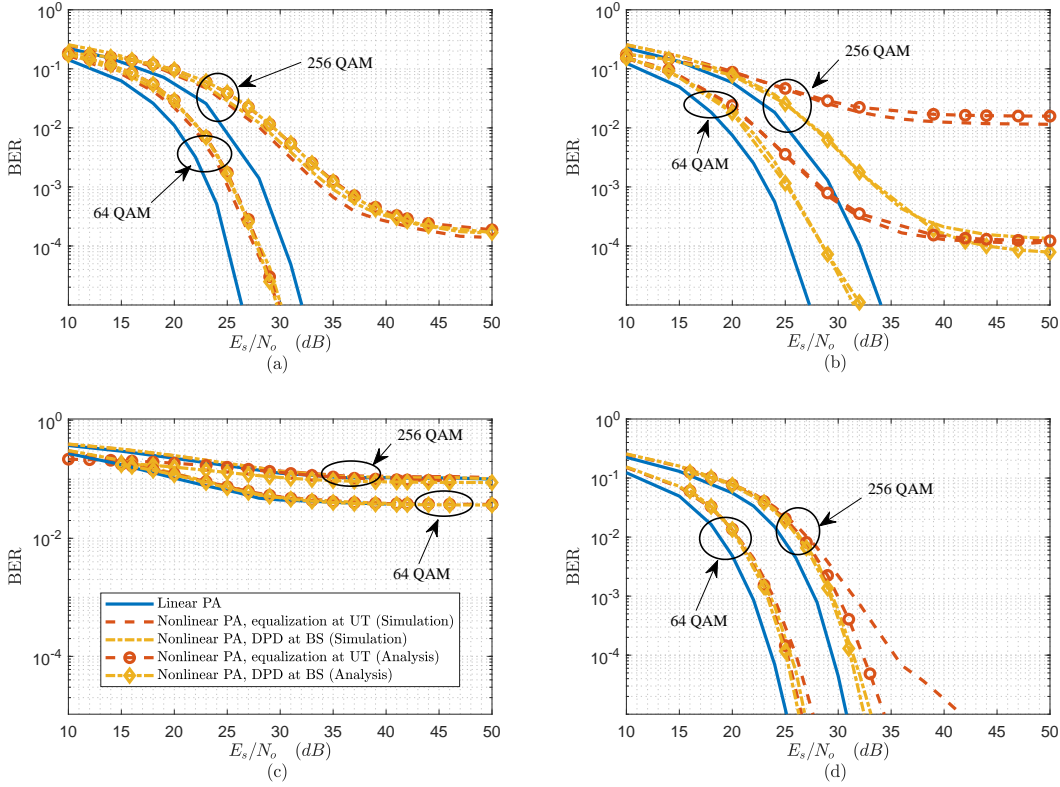


Fig. 7. Analytical and simulation results for average BER obtained for different array architectures (a) fully connected (b) partially connected with GEB (c) partially connected with phase only subarray (d) fully digital beamforming for 64 and 256 QAM

In subarray with GEB, improvement in the performance becomes more apparent. For both 256 and 64 QAM, equalization at UT cannot prevent error floor. However, by employing DPD, error floor in 64 QAM is reduced to a significantly low level. Furthermore, error floor of subarray with GEB for 256 QAM is slightly lower than that of fully connected beamforming.

## VII. CONCLUSION AND FUTURE WORKS

In this work, we presented a comprehensive performance analysis framework for evaluation of massive MIMO systems, which are subject to PA nonlinearities for different beamforming

architectures. In addition, anti-beamforming based indirect learning approach is adopted in design of DPD and a post-equalization method is proposed. GEB based sub-array design is proposed in order to provide sufficient inter-group interference in analog domain, which cannot be achieved by conventional DFT beamformer. Both in-band and out-of-band radiation patterns are considered for different array architectures. Significant amount of OOB radiation results due to nonlinear distortion caused by PA's; however, in band pattern is not significantly affected. Proposed DPD can achieve OOB reduction for all array architectures except fully connected architecture. DPD design for fully connected architecture that considers the connectivity of this architecture remains as a future work. GMI metric is employed in order to compare array architectures in terms of AIR. Observations on AIR performances are in compliance with that of OOB radiation. It can be observed that fully digital beamforming architecture is robust against PA nonlinearities since maximum capacity can be achieved by using only linear equalization at the receiver. In addition, fully connected architecture provides acceptable performance under PA nonlinearities even if its OOB radiation cannot be reduced. On the other hand, DFT beamformer suffers from significant performance degradation even with linear PA due to poor performance of analog beamformer design. Lastly, analytical BER expressions are derived for different array architectures based on spatio-temporal multidimensional Bussgang decomposition and BER performances of array architectures are compared. Sub-array with DFT beamformer exhibits poor performance while fully digital beamformer provides the best possible performance. Proposed sub-array with GEB outperforms fully connected architecture for higher order modulations however lower order modulations fully connected architecture is more beneficial. As a result, sub-array with GEB provides trade-off between OOB suppression and BER performance. However, fully connected architecture would have promising performance with proper DPD design.

## REFERENCES

- [1] S. Rangan, T. S. Rappaport, and E. Erkip, "Millimeter-wave cellular wireless networks: Potentials and challenges," *Proc. IEEE*, vol. 102, no. 3, pp. 366–385, Feb. 2014.
- [2] Z. Pi and F. Khan, "An introduction to millimeter-wave mobile broadband systems," *IEEE Commun. Mag.*, vol. 49, no. 6, pp. 101–107, Jun. 2011.
- [3] E. G. Larsson, O. Edfors, F. Tufvesson, and T. L. Marzetta, "Massive mimo for next generation wireless systems," *IEEE Commun. Mag.*, vol. 52, no. 2, pp. 186–195, Feb. 2014.
- [4] T. S. Rappaport, S. Sun, R. Mayzus, H. Zhao, Y. Azar, K. Wang, G. N. Wong, J. K. Schulz, M. Samimi, and F. Gutierrez, "Millimeter wave mobile communications for 5g cellular: It will work!" *IEEE Access*, vol. 1, pp. 335–349, May 2013.
- [5] F. Boccardi, R. W. Heath, A. Lozano, T. L. Marzetta, and P. Popovski, "Five disruptive technology directions for 5G," *IEEE Commun. Mag.*, vol. 52, no. 2, pp. 74–80, Feb. 2014.
- [6] Q. H. Spencer, A. L. Swindlehurst, and M. Haardt, "Zero-forcing methods for downlink spatial multiplexing in multiuser mimo channels," *IEEE Trans. on Signal Process.*, vol. 52, no. 2, pp. 461–471, Jan. 2004.
- [7] A. F. Molisch, V. V. Ratnam, S. Han, Z. Li, S. L. H. Nguyen, L. Li, and K. Haneda, "Hybrid beamforming for massive mimo: A survey," *IEEE Commun. Mag.*, vol. 55, no. 9, pp. 134–141, Sep. 2017.
- [8] S. Han, C. I, Z. Xu, and C. Rowell, "Large-scale antenna systems with hybrid analog and digital beamforming for millimeter wave 5g," *IEEE Commun. Mag.*, vol. 53, no. 1, pp. 186–194, Jan. 2015.
- [9] S. Payami, M. Ghoraiishi, M. Dianati, and M. Sellathurai, "Hybrid beamforming with a reduced number of phase shifters for massive mimo systems," *IEEE Trans. Veh. Technol.*, vol. 67, no. 6, pp. 4843–4851, Feb. 2018.
- [10] A. Adhikary, J. Nam, J. Ahn, and G. Caire, "Joint spatial division and multiplexingthe large-scale array regime," *IEEE Trans. Inf. Theory*, vol. 59, no. 10, pp. 6441–6463, Jun. 2013.
- [11] G. M. Guvensen and E. Ayanoglu, "A generalized framework on beamformer design and csi acquisition for single-carrier massive mimo systems in millimeter wave channels," in *Proc. IEEE Globecom*, Dec. 2016, pp. 1–7.
- [12] A. Kurt and G. M. Guvensen, "An efficient hybrid beamforming and channel acquisition for wideband mm-wave massive mimo channels," in *Proc. IEEE Int. Conf. Commun*, May 2019, pp. 1–7.
- [13] A. Adhikary, E. Al Safadi, M. K. Samimi, R. Wang, G. Caire, T. S. Rappaport, and A. F. Molisch, "Joint spatial division and multiplexing for mm-wave channels," *IEEE J. Sel. Areas Commun.*, vol. 32, no. 6, pp. 1239–1255, May 2014.
- [14] N. Peccarelli, B. James, R. Irazoqui, J. Metcalf, C. Fulton, and M. Yeary, "Survey: Characterization and mitigation of spatial/spectral interferers and transceiver nonlinearities for 5g mimo systems," *IEEE Trans. Microw. Theory Techn.*, vol. 67, no. 7, pp. 2829–2846, May 2019.
- [15] C. Molln, U. Gustavsson, T. Eriksson, and E. G. Larsson, "Out-of-band radiation measure for mimo arrays with beamformed transmission," in *Proc. IEEE Int. Conf. Commun*, May 2016, pp. 1–6.

- [16] C. Mollen, E. G. Larsson, U. Gustavsson, T. Eriksson, and R. W. Heath, "Out-of-band radiation from large antenna arrays," *IEEE Commun. Mag.*, vol. 56, no. 4, pp. 196–203, Apr. 2018.
- [17] C. Mollen, U. Gustavsson, T. Eriksson, and E. G. Larsson, "Spatial characteristics of distortion radiated from antenna arrays with transceiver nonlinearities," *IEEE Trans. Wireless Commun.*, vol. 17, no. 10, pp. 6663–6679, Aug. 2018.
- [18] M. Abdelaziz, L. Anttila, A. Brihuega, F. Tufvesson, and M. Valkama, "Digital predistortion for hybrid mimo transmitters," *IEEE J. Sel. Topics Signal Process.*, vol. 12, no. 3, pp. 445–454, Apr. 2018.
- [19] H. Moazzen, A. Mohammadi, and M. Majidi, "Performance analysis of linear precoded mu-mimo-ofdm systems with nonlinear power amplifiers and correlated channel," *IEEE Trans. Commun.*, vol. 67, no. 10, pp. 6753–6765, Oct 2019.
- [20] J. Guerreiro, R. Dinis, and P. Montezuma, "Analytical performance evaluation of precoding techniques for nonlinear massive mimo systems with channel estimation errors," *IEEE Trans. Commun.*, vol. 66, no. 4, pp. 1440–1451, Dec. 2018.
- [21] H. Hemesi, A. Abdipour, and A. Mohammadi, "Analytical modeling of mimo-ofdm system in the presence of nonlinear power amplifier with memory," *IEEE Trans. Commun.*, vol. 61, no. 1, pp. 155–163, Nov. 2013.
- [22] P. Aggarwal and V. A. Bohara, "End-to-end theoretical evaluation of a nonlinear mimo-ofdm system in the presence of digital predistorter," *IEEE Syst. J.*, vol. 13, no. 3, pp. 2309–2319, Oct. 2019.
- [23] L. Liu, W. Chen, L. Ma, and H. Sun, "Single-pa-feedback digital predistortion for beamforming mimo transmitter," in *Proc. IEEE Int. Conf. Microw. Millimeter Wave Technol.*, vol. 2, Jun. 2016, pp. 573–575.
- [24] M. B. Salman and G. M. Guvensen, "On the effects of pa nonlinearities for hybrid beamforming based wideband massive mimo systems," in *Proc. IEEE Int. Conf. Commun.*, accepted for IEEE ICC Wireless Communication Semposium.
- [25] E. Bjrnson, J. Hoydis, M. Kountouris, and M. Debbah, "Massive mimo systems with non-ideal hardware: Energy efficiency, estimation, and capacity limits," *IEEE Trans. Inf. Theory*, vol. 60, no. 11, pp. 7112–7139, Sep. 2014.
- [26] G. Ungerboeck, "Channel coding with multilevel/phase signals," *IEEE Trans. Inf. Theory*, vol. 28, no. 1, pp. 55–67, Jan. 1982.
- [27] A. Lapidoth, "Mismatched decoding and the multiple-access channel," *IEEE Trans. Inf. Theory*, vol. 42, no. 5, pp. 1439–1452, Sep. 1996.
- [28] A. Modenini, F. Rusek, and G. Colavolpe, "Optimal transmit filters for isi channels under channel shortening detection," *IEEE Transactions on Communications*, vol. 61, no. 12, pp. 4997–5005, Dec. 2013.
- [29] Z. Glgn and A. . Ylmaz, "Detection schemes for high order  $m$  -ary qam under transmit nonlinearities," *IEEE Trans. Commun.*, vol. 67, no. 7, pp. 4825–4834, Mar. 2019.
- [30] Y. Zou, O. Raeesi, L. Antilla, A. Hakkarainen, J. Vieira, F. Tufvesson, Q. Cui, and M. Valkama, "Impact of power amplifier nonlinearities in multi-user massive mimo downlink," in *Proc. IEEE Globecom Workshops*, Dec. 2015, pp. 1–7.
- [31] D. R. Morgan, Z. Ma, J. Kim, M. G. Zierdt, and J. Pastalan, "A generalized memory polynomial model for digital predistortion of rf power amplifiers," *IEEE Trans. Signal Process.*, vol. 54, no. 10, pp. 3852–3860, Sep. 2006.
- [32] Ericsson, "Further elaboration on pa models for nr," Ericsson AB, Stockholm, Sweden, Tech. Rep., Aug. 2016. [Online]. Available: [www.3gpp.org/ftp/tsg\\_ran/WG4\\_Radio/TSGR4\\_80/Docs/R4-165901.zip](http://www.3gpp.org/ftp/tsg_ran/WG4_Radio/TSGR4_80/Docs/R4-165901.zip)